



HAL
open science

Multiscale modelling of the composite reinforced foam core of a 3D sandwich structure

J. Guilleminot, S. Comas-Cardona, D. Kondo, C. Binetruy, P. Krawczak

► **To cite this version:**

J. Guilleminot, S. Comas-Cardona, D. Kondo, C. Binetruy, P. Krawczak. Multiscale modelling of the composite reinforced foam core of a 3D sandwich structure. *Composites Science and Technology*, 2009, 68 (7-8), pp.1777. 10.1016/j.compscitech.2008.02.005 . hal-00585784

HAL Id: hal-00585784

<https://hal.science/hal-00585784>

Submitted on 14 Apr 2011

HAL is a multi-disciplinary open access archive for the deposit and dissemination of scientific research documents, whether they are published or not. The documents may come from teaching and research institutions in France or abroad, or from public or private research centers.

L'archive ouverte pluridisciplinaire **HAL**, est destinée au dépôt et à la diffusion de documents scientifiques de niveau recherche, publiés ou non, émanant des établissements d'enseignement et de recherche français ou étrangers, des laboratoires publics ou privés.

Accepted Manuscript

Multiscale modelling of the composite reinforced foam core of a 3D sandwich structure

J. Guillemot, S. Comas-Cardona, D. Kondo, C. Binetruy, P. Krawczak

PII: S0266-3538(08)00040-7
DOI: [10.1016/j.compscitech.2008.02.005](https://doi.org/10.1016/j.compscitech.2008.02.005)
Reference: CSTE 3965

To appear in: *Composites Science and Technology*

Received Date: 1 August 2007
Revised Date: 18 January 2008
Accepted Date: 4 February 2008

Please cite this article as: Guillemot, J., Comas-Cardona, S., Kondo, D., Binetruy, C., Krawczak, P., Multiscale modelling of the composite reinforced foam core of a 3D sandwich structure, *Composites Science and Technology* (2008), doi: [10.1016/j.compscitech.2008.02.005](https://doi.org/10.1016/j.compscitech.2008.02.005)

This is a PDF file of an unedited manuscript that has been accepted for publication. As a service to our customers we are providing this early version of the manuscript. The manuscript will undergo copyediting, typesetting, and review of the resulting proof before it is published in its final form. Please note that during the production process errors may be discovered which could affect the content, and all legal disclaimers that apply to the journal pertain.



Multiscale modelling of the composite reinforced foam core of a 3D sandwich structure

J. Guillemot^a, S. Comas-Cardona^a, D. Kondo^b, C. Binetruy^a,
P. Krawczak^a

^a*Ecole des Mines de Douai, Polymers and Composites Technology & Mechanical Engineering Department, 941 rue Charles Bourseul, BP 10838, 59508 Douai Cedex, France*

^b*Université des Sciences et Technologies de Lille, Laboratoire de Mécanique de Lille-UMR CNRS 8107, Cité Scientifique, Bd. Paul Langevin, 59655 Villeneuve d'Ascq Cedex, France*

Abstract

A key objective dealing with 3D sandwich structures is to maximize the through-thickness stiffness, the strength of the core and the core to faces adhesion. The Napco[®] technology was especially designed for improving such material properties and is under investigation in this paper. In particular, the potential of the process is characterized using a micromechanical modelling combined to a parametric probabilistic model. An experimental analysis is further detailed and validates the theoretical estimates of the core-related elastic properties. It is readily shown that the technology is able to produce parts with significantly improved mechanical properties. Finally, thanks to the probabilistic aspect of the modelling, the study allows to establish a link between the randomness of the process and the uncertainties of the final mechanical properties. Thus, the present approach can be used to optimize the technology as well as to properly design structures.

Key words: A. Sandwich, B. Mechanical properties, C. Multiscale modeling, C. Sandwich structures

Email address: guillemot@ensm-douai.fr (J. Guillemot).

1 Introduction

1.1 General introduction

The high strength, high specific weight and durability of sandwich composites make them highly attractive for aerospace, marine and ground transportation applications. Therefore, sandwich components have been successfully introduced to several applications such as roof panels in train and bus structures, front cabins of high-speed locomotives, interior panels... Minimizing the weight of a structure is becoming a common key design objective as it allows many options such as higher speed, longer range, larger payloads, less engine power and better operating economy. The sandwich material must be light whilst remaining economically viable. Moreover, high shear strength and modulus are also major considerations and the core should have good load bearing capacity and sufficient compressive strength to withstand local indentative loads. Finally, good thermal stability as well as good fatigue resistance is usually required.

In order to increase the load capacity of the sandwich construction without penalizing its lightness, it is then desirable to maximize the through-thickness stiffness and strength of the core. One strategy of achieving this is to add through-thickness reinforcement to the core, with the ends of the reinforcement material embedded in composite facings. The best option is to have a continuous 3D reinforcement to increase the delamination strength and toughness between facings and core. In recent years several investigators have considered a number of innovative designs to improve the strength of foam cores such as 3D weaving [1], 3D Z-pins embedded in foam [14], stitch bonding [6] [10] and hollow integrated core sandwich [5]. Usually these solutions lead to a decrease of production rate and an increase of part cost. An alternative is the patented Napco[®] technology which produces, in a continuous way, 3D tailored sandwich structures while maintaining a production efficiency [9].

The main objective of this study is to show the potential of such a manufacturing process by evaluating the resulting enhancement of some mechanical properties. For this purpose, a micromechanical approach is first proposed and integrates the anisotropy (due to the through-thickness reinforcements) of the reinforced foam core. Predictions of this multiscale modelling are then compared and discussed with respect to an experimental database which is also briefly described. Finally, in order to take into account the randomness of both the elementary constituents and the manufacturing process, a parametric probabilistic model is introduced.

2 Napco[®] technology

The Napco[®] technology is a manufacturing process of 3D fibrous structures and 3D dry sandwich composites in which the facing fabrics and core are integrated together in one construction. The sandwich construction is based on needle punching (Fig. 1). The through-thickness reinforcement is obtained from regular fabrics such as chopped strand mats or continuous fiber mats. A multi-needle arrangement, set at a desired pattern and density, penetrates the assembly of glass fabric layers and foam core on both sides (Fig. 2). During this process, needles catch and pull glass strands from the facings and carry them through the rigid foam, creating straight reinforcements perpendicular to the skins (see Figs. (1) and (2)). A part of the yarn is kept inside the facings, the rest being embedded within the foam core. Thus, note that the Napco[®] technology basically differs from the stitching technology, where the fibers do not come from the skin material. As the needles are withdrawn, fibers remain inside the core. Then the sandwich panel assembly is advanced by a desired spacing to produce the next set of vertical pile yarns.

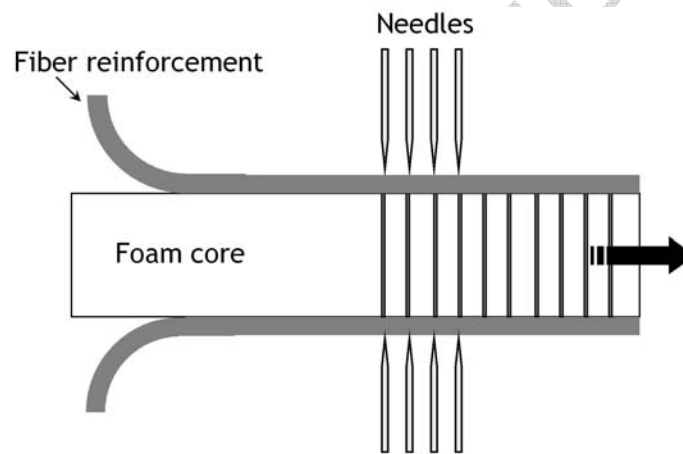


Figure 1. Schematic illustration of the Napco[®] technology

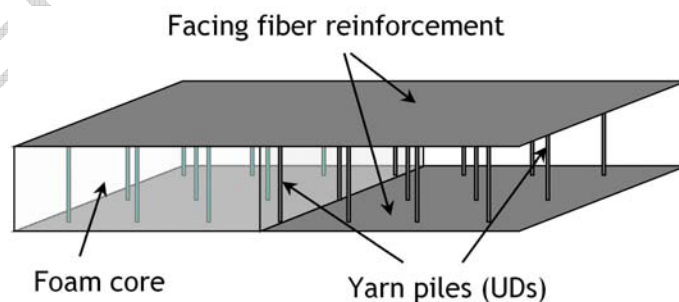


Figure 2. Schematic illustration of the 3D sandwich construction yielded by the Napco[®] technology

Once the 3D sandwich preform is produced, it can be impregnated by a liquid resin using of any composite molding technique. Closed-mold methods (Liquid

Composite Molding) and continuous compression molding are found to be appropriate. For those technologies, it has been noticed that the transverse pile yarns are properly impregnated. In addition, they help to balance resin flow on both sides of the sandwich.

3 Micromechanical modelling

The reinforced foam core is made up of a linearly elastic matrix (the polyurethane foam) reinforced by unidirectional composites (UDs), as shown on figure 3. The matrix is considered as isotropic while the through-thickness re-

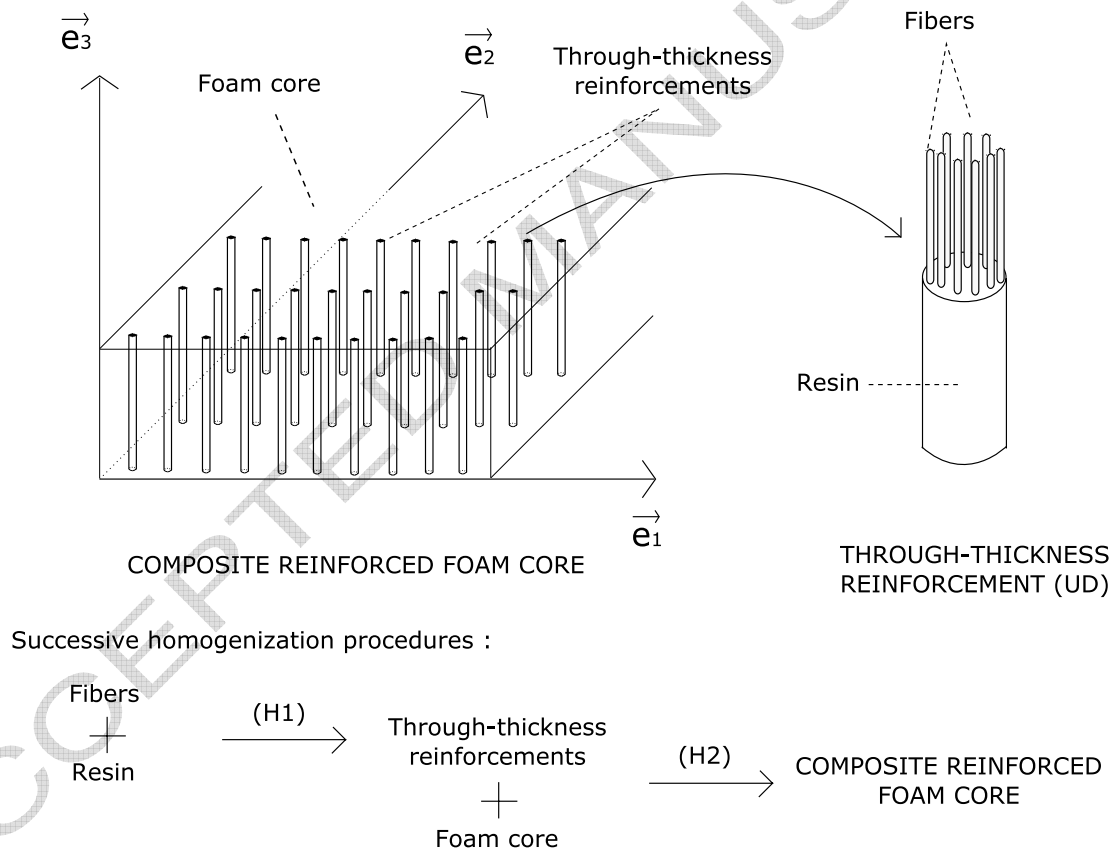


Figure 3. Modelling of the composite reinforced foam core.

inforcements are approximated as long circular transversely isotropic cylinders. Hence, the overall mechanical response of the composite is transversely isotropic.

3.1 Base tensors for transversely isotropic materials

We first recall some notations of tensor algebra corresponding to transversally isotropy. The basic idea was introduced by Walpole [15] and was recently summarized in [3]. Any transversely isotropic fourth-order tensor \mathbb{A} can be expressed in terms of six basic fourth-order tensors defined as:

$$\begin{aligned}
 \mathbb{E}_L &= \underline{n} \otimes \underline{n} \otimes \underline{n} \otimes \underline{n} \\
 \mathbb{J}_T &= \frac{1}{2} \mathbf{i}_T \otimes \mathbf{i}_T \\
 \mathbb{F} &= \frac{1}{\sqrt{2}} \mathbf{i}_T \otimes \underline{n} \otimes \underline{n} \\
 {}^T\mathbb{F} &\text{ such as } ({}^T F)_{ijkl} = (F)_{klij} \\
 \mathbb{K}_T &= \mathbb{I}_T - \mathbb{J}_T \\
 \mathbb{K}_L &= \mathbb{I} - \frac{1}{3} \mathbf{i} \otimes \mathbf{i} - \mathbb{K}_T - \mathbb{K}_E
 \end{aligned} \tag{1}$$

where:

- the unit normal \underline{n} defines the axis of transverse isotropy. In this study, according to figure (3), one has $\underline{n} = \underline{e}_3$;
- \mathbf{i}_T and \mathbb{I}_T denote the second and fourth-order identity tensors in the transverse plane and are respectively given by:

$$\begin{aligned}
 \mathbf{i}_T &= \mathbf{i} - \underline{n} \otimes \underline{n} \\
 \mathbb{I}_T &= \mathbb{I} + \underline{n} \otimes \underline{n} \otimes \underline{n} \otimes \underline{n} - 2 [\underline{n} \otimes \mathbf{i} \otimes \underline{n}]^{(\text{sym})}
 \end{aligned} \tag{2}$$

where the superscript (sym) denotes the double symmetrization operator defined as:

$$\left(\mathbb{A}^{(\text{sym})} \right)_{ijkl} = (A_{ijkl} + A_{jikl} + A_{ijlk} + A_{jilk}) / 4 \tag{3}$$

\mathbf{i} and \mathbb{I} are the second and symmetric fourth-order identity tensors respectively ($i_{ij} = \delta_{ij}$ and $2I_{ijkl} = \delta_{ik}\delta_{jl} + \delta_{il}\delta_{jk}$, where δ_{ij} is the Kronecker delta);

- \mathbb{K}_E is defined as:

$$\mathbb{K}_E = \frac{1}{6} (2\underline{n} \otimes \underline{n} - \mathbf{i}_T) \otimes (2\underline{n} \otimes \underline{n} - \mathbf{i}_T) \tag{4}$$

Then, the decomposition

$$\mathbb{A} = \alpha \mathbb{E}_L + \beta \mathbb{J}_T + \gamma \mathbb{F} + \gamma' {}^T\mathbb{F} + \delta \mathbb{K}_T + \delta' \mathbb{K}_L \tag{5}$$

can be written in the following symbolic form:

$$\mathbb{A} = \{ \underline{a}, \delta, \delta' \} \tag{6}$$

where the matrix \underline{a} is defined as ($\gamma = \gamma'$ when \mathbb{A} is symmetric):

$$\underline{a} = \begin{bmatrix} \alpha & \gamma \\ \gamma' & \beta \end{bmatrix} \quad (7)$$

Thus, the following basic tensorial operations take the simple forms:

$$\begin{aligned} \mathbb{A}_1 + \mathbb{A}_2 &= \{\underline{a}_1, \delta_1, \delta'_1\} + \{\underline{a}_2, \delta_2, \delta'_2\} = \{\underline{a}_1 + \underline{a}_2, \delta_1 + \delta_2, \delta'_1 + \delta'_2\} \\ \mathbb{A}_1 : \mathbb{A}_2 &= \{\underline{a}_1, \delta_1, \delta'_1\} : \{\underline{a}_2, \delta_2, \delta'_2\} = \{\underline{a}_1 \cdot \underline{a}_2, \delta_1 \delta_2, \delta'_1 \delta'_2\} \\ \mathbb{A}^{-1} &= \{\underline{a}, \delta, \delta'\}^{-1} = \{\underline{a}^{-1}, 1/\delta, 1/\delta'\} \end{aligned} \quad (8)$$

When \mathbb{A} corresponds to a fourth-order symmetric stiffness tensor, the parameters involved in the decomposition (5) can be written in terms of the well known engineering constants:

$$\begin{aligned} \alpha &= E^l + 4(\nu^l)^2 K, \quad \beta = 2K, \quad \gamma = \gamma' = 2\sqrt{2}\nu^l K \\ \delta &= 2\mu^t, \quad \delta' = 2\mu^l \end{aligned} \quad (9)$$

where E^l , μ^l and ν^l are the longitudinal Young's modulus, shear modulus and Poisson ratio respectively. μ^t and K are the transverse shear modulus and the in-plane bulk modulus respectively. In this study, the longitudinal direction (denoted by the superscript l) coincides with the through-thickness orientation of the sandwich.

3.2 Micromechanical analysis

3.2.1 Principle

In order to assess the overall properties of the material, two successive homogenization procedures are carried out (the different scales being assumed to be well separated) as follows (see Fig. (3)):

- the first one, denoted by (H1), is performed at the scale of the unidirectional composite and provides the estimate of the effective stiffness tensor of the UD, denoted by $\tilde{\mathbb{C}}$;
- the second one, denoted by (H2), is carried out at the upper scale (the UDs being then considered as the inhomogeneities) and allows us to estimate the macroscopic stiffness tensor $\tilde{\tilde{\mathbb{C}}}$ of the composite reinforced foam core.

Note that (H1) is basically a specific case of (H2) and can be achieved substituting the corresponding properties (considering an isotropic matrix reinforced

by aligned isotropic fibers) in the results that will be given for the second homogenization procedure. The aim of this section is to estimate the macroscopic mechanical properties of the foam reinforced by the through-thickness UD. For this purpose, we consider the Mori-Tanaka estimate (i.e. the matrix is considered as the reference medium and is subjected to its own stress, see [2] [3] [7]), which allows to take into account the interactions between the inhomogeneities. The choice of this homogenization scheme is justified by the “matrix-inclusion” morphology of the studied material. In general, the validity of this approach corresponds to a reinforcement volume fraction c_{H_2} such that $c_{H_2} < 20\%$ (note that this validity range may be reduced or extended, depending in particular on the contrast between the constituents as well as on the required accuracy [3]). In the case of the two-phase composite considered here, the overall stiffness tensor $\tilde{\mathbb{C}}$ is then given by:

$$\tilde{\mathbb{C}}^{\text{MT}} = \mathbb{C}_1 + c_{H_2} (\tilde{\mathbb{C}} - \mathbb{C}_1) : \mathbb{A}_2^{\text{MT}} \quad (10)$$

where $\tilde{\mathbb{C}}^{\text{MT}}$ is the macroscopic stiffness tensor estimated by means of the Mori-Tanaka scheme, \mathbb{C}_1 and $\tilde{\mathbb{C}}$ are the stiffness tensors of the matrix and the inhomogeneity respectively. c_{H_2} denotes the volume fraction of reinforcing material and \mathbb{A}_2^{MT} is the strain concentration tensor for the inhomogeneity, defined as:

$$\mathbb{A}_2^{\text{MT}} = [\mathbb{I} + \mathbb{P}_1^2 : \Delta\mathbb{C}]^{-1} : \left[(1 - c_{H_2}) \mathbb{I} + c_{H_2} [\mathbb{I} + \mathbb{P}_1^2 : \Delta\mathbb{C}]^{-1} \right]^{-1} \quad (11)$$

where $\Delta\mathbb{C} = \tilde{\mathbb{C}} - \mathbb{C}_1$ and \mathbb{P}_1^2 is the Hill tensor corresponding to the inhomogeneity 2 (that is, the through-thickness reinforcement) embedded in the matrix 1. We further recall that:

$$\mathbb{P}_1^2 = \mathbb{P}_1^2|_{\text{MT}} = \mathbb{S}_{\text{ESH}} : [\mathbb{C}_1]^{-1} \quad (12)$$

where \mathbb{S}_{ESH} is the Eshelby tensor of the inhomogeneity. It is readily seen from Eq. (12) that the Hill tensor basically depends on both the geometry of the inhomogeneity (via \mathbb{S}_{ESH}) and the mechanical properties of the reference medium (here, the matrix).

3.2.2 Determination of the macroscopic properties

In the case of the UD (classically modelled as ellipsoidal inclusions with an infinite aspect ratio: $w = L/d \rightarrow \infty$, where L and d are the length and the diameter of the inclusion), oriented in the direction \underline{n} , it can be shown that the Hill tensor takes the form (see [3]):

$$\mathbb{P}_1^2 = \frac{1}{2(K_1 + \mu_1)} \mathbb{J}_T + \frac{1}{4\mu_1} \frac{K_1 + 2\mu_1}{K_1 + \mu_1} \mathbb{K}_T + \frac{1}{4\mu_1} \mathbb{K}_L \quad (13)$$

where K_1 and μ_1 are the in-plane bulk modulus and shear modulus of the matrix respectively. Taking into account Eq. (6), Eq. (13) is then rewritten as:

$$\mathbb{P}_1^2 = \left\{ \left[\begin{array}{cc} 0 & 0 \\ 0 & 1/2(K_1 + \mu_1) \end{array} \right], \frac{1}{4\mu_1} \frac{K_1 + 2\mu_1}{K_1 + \mu_1}, \frac{1}{4\mu_1} \right\} \quad (14)$$

Furthermore, one has:

$$\mathbb{I} = \left\{ \left[\begin{array}{cc} 1 & 0 \\ 0 & 1 \end{array} \right], 1, 1 \right\} \quad (15)$$

Combining (6) and (9) yields the expression of the stiffness tensor for the transversely isotropic reinforcing material:

$$\tilde{\mathbb{C}} = \left\{ \left[\begin{array}{cc} \tilde{E}^l + 4(\tilde{\nu}^l)^2 \tilde{K} & 2\sqrt{2}\tilde{\nu}^l \tilde{K} \\ 2\sqrt{2}\tilde{\nu}^l \tilde{K} & 2\tilde{K} \end{array} \right], 2\tilde{\mu}^t, 2\tilde{\mu}^l \right\} \quad (16)$$

where

$$\tilde{K} = \frac{1}{2} \frac{\tilde{E}^t \tilde{E}^l}{(1 - \tilde{\nu}^t) \tilde{E}^l - 2(\tilde{\nu}^l)^2 \tilde{E}^t} \quad (17)$$

We recall that the elastic properties involved in the above decomposition are obtained from the first homogenization (H1).

The stiffness tensor of the isotropic matrix is easily obtained by substituting $\tilde{E}^l = \tilde{E}^t = E_1$, $\tilde{\nu}^l = \tilde{\nu}^t = \nu_1$ and $\tilde{\mu}^l = \tilde{\mu}^t = \mu_1$ into (16), that is:

$$\mathbb{C}_1 = \left\{ \left[\begin{array}{cc} E_1 + 4(\nu_1)^2 K_1 & 2\sqrt{2}\nu_1 K_1 \\ 2\sqrt{2}\nu_1 K_1 & 2K_1 \end{array} \right], 2\mu_1, 2\mu_1 \right\} \quad (18)$$

where

$$K_1 = k_1 + \frac{\mu_1}{3} \quad (19)$$

and k_1 is the three dimensional bulk modulus of the matrix.

Since the macroscopic response of the material is transversely isotropic, one has:

$$\tilde{\mathbb{C}} = \left\{ \left[\begin{array}{cc} \tilde{\alpha} & \tilde{\gamma} \\ \tilde{\gamma} & \tilde{\beta} \end{array} \right], \tilde{\delta}, \tilde{\delta}' \right\} \quad (20)$$

The effective properties involved in the decomposition (20) can be easily estimated by substituting Eqs. (14), (16), (18) and (20) into Eq. (10) and making use of Eq. (8).

For instance, in the case of the overall transverse shear modulus (which is

critical for such materials) $\widetilde{\mu}^t$, one has:

$$\widetilde{\mu}^t = \mu_1 + \frac{c_{H_2} (\widetilde{\mu}^t - \mu_1)}{b_1 b_2} \quad (21)$$

where

$$\begin{aligned} b_1 &= 1 + (k_1 + 7\mu_1/3) (\widetilde{\mu}^t - \mu_1) / \{2\mu_1 (k_1 + 4\mu_1/3)\} \\ b_2 &= 1 - c_{H_2} + c_{H_2} / \left\{ 1 + (k_1 + 7\mu_1/3) (\widetilde{\mu}^t - \mu_1) / \{2\mu_1 (k_1 + 4\mu_1/3)\} \right\} \end{aligned} \quad (22)$$

It is readily seen that $\widetilde{\mu}^t \rightarrow \mu_1$ when $c_{H_2} \rightarrow 0$ and $\widetilde{\mu}^t \rightarrow \widetilde{\mu}^t$ when $c_{H_2} \rightarrow 1$. Finally, note that under dilute conditions (i.e. $c_{H_2} \rightarrow 0$) and for an isotropic reinforcing material (so that: $\widetilde{\mu}^t = \mu^f$, where μ^f is the shear modulus of the reinforcing fiber), Eq. (21) reads:

$$\frac{\widetilde{\mu}^t}{\mu_1} \Big|_{\text{Dilute}} \approx 1 + \frac{c_{H_2}}{\mu_1 / (\mu^f - \mu_1) + (k_1 + 7\mu_1/3) / (2k_1 + 8\mu_1/3)} \quad (23)$$

which is exactly the result provided by Christensen (see [4], p. 89).

4 Experimental validation

4.1 Sandwich manufacturing

The sandwich preforms are made using the Napco[®] technology with a polyurethane foam core (density of 40 kg.m⁻³), two facings made of 1 ply of chopped strand glass mat (areal weight of 450 g.m⁻²). The final panel is molded using continuous compression molding with unsaturated polyester resin. Three different types of needle pattern have been used to create different pile yarns (UDs) densities in the final sandwich structure (Tab. (1)).

4.2 Modelling data

In this section, we consider elementary constituents the properties of which are listed in Tab. (2).

The first homogenization procedure (H1) is performed (with a fiber volume

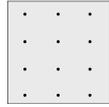
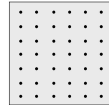
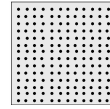
Sandwich panel #	1	2	3
Top view			
Average total thickness (mm)	16.7	16.4	16.2
Average core thickness (mm)	14.5	14.3	14.3
Distance between UD's (mm)	15×15	8×8	4×4
Volume fraction of UD's wrt foam core c_{H_2}	1.2%	4.3%	9.4%

Table 1

Sandwich panels specifications

Constituents	Elastic properties
Polyester resin	$E = 4\,000$ MPa, $\nu = 0.4$
E-Glass fibers	$E = 73\,000$ MPa, $\nu = 0.22$
Polyurethane foam	$E = 9.2$ MPa, $\nu = 0$

Table 2

Elastic properties of the elementary constituents.

fraction equal to the mean experimental value: $c_{H_1} = 4.1\%$) and provides the overall elastic properties of the UD, listed in Tab. (3) (we recall that the methodology described in the previous section is used for that purpose).

Overall properties of the UD
$\tilde{E}^l = 6\,834$ MPa
$\tilde{\mu}^t = 1\,524$ MPa
$\tilde{\mu}^l = 1\,538$ MPa
$\tilde{K} = 14\,900$ Mpa
$\tilde{\nu}^l = 0.39$

Table 3

Overall properties of the unidirectional composite.

In order to accurately compare the estimates with experimental data, we further introduce a correction index, denoted by r and defined as the mean value of the ratio between the predictions and the experimental results for a given elastic property T :

$$r_T = \frac{1}{N} \sum_{i=1}^N \frac{T_i^{Est.}}{T_i^{Exp.}} \quad (24)$$

where $T_i^{Est.}$ and $T_i^{Exp.}$ are the i -th estimated and experimental values respectively, N is the total number of observations of T (one observation basically corresponds to one volume fraction in through-thickness reinforcements). The i -th corrected estimate is then defined as:

$$T_i^{Corr.} = \frac{T_i^{Est.}}{r_T} \quad (25)$$

4.3 Results and discussion

Compression between parallel plates and three-point bending tests were performed on a material-testing machine (Zwick) mounted with a 100kN-force cell.

4.3.1 Case of the overall longitudinal (through-thickness) Young's modulus \widetilde{E}^l

The panels have been characterized in compression following the NF T 54-602 standard. Five samples were cut in each of the three panels. The compression speed of the top compression platen was $1.6 \text{ mm} \cdot \text{min}^{-1}$. The compression moduli were calculated from the experimental stress-strain curves. Fig. (4) shows a comparison between the experimental data and the simulations (obtained from Eqs. (9) and (20)). It is seen that:

- the evolution of the elastic property is quite well predicted;
- the magnitude of the modulus is well estimated, even by the non corrected formulation.

The estimate of the overall longitudinal Young's modulus as a function of the volume fractions in both the UD's and the foam core is illustrated in Fig. 5. The figure shows that:

- the overall modulus is highly sensitive to the volume fraction in through-thickness reinforcements c_{H_2} as well as to the volume fraction c_{H_1} (within the UD's);
- a significant increase of the property can be obtained, even at a rather small volume fraction c_{H_2} (and especially, if c_{H_1} can be increased by enhanced carriage of fibers by needles).

**Effective longitudinal
Young's modulus, in MPa**

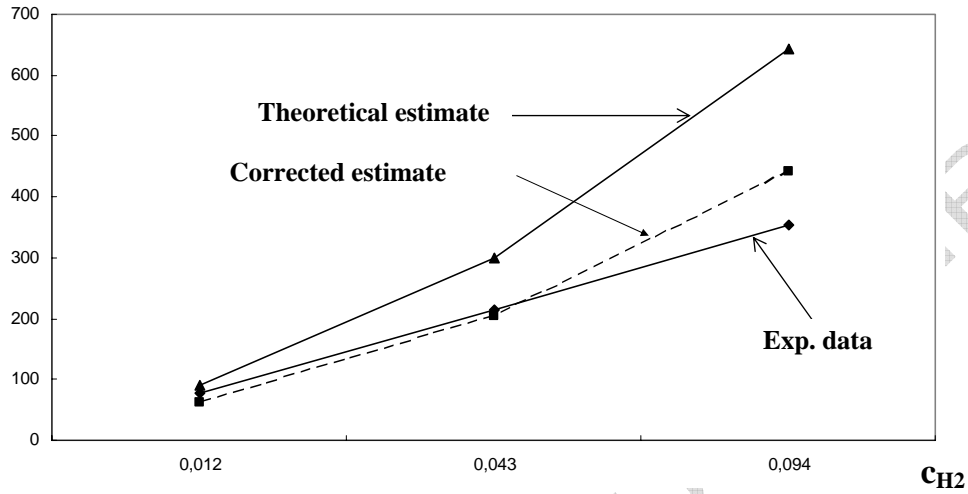


Figure 4. Comparison between exp. data and micromechanical predictions. Case of the overall longitudinal Young's modulus \widetilde{E}^l .

4.3.2 Case of the overall transverse shear modulus $\widetilde{\mu}^t$

The panels have also been submitted to three-point bending test following the NF T 54-606 standard. Since two span lengths were used (300 and 450 mm), ten samples were cut in each panel. The cross-head speed was setup accordingly to the standard to $0.8 \text{ mm}\cdot\text{min}^{-1}$. Fig. (6) shows a comparison between the experimental data and the simulations. It is seen that:

- the evolution of the elastic property is well predicted;
- the magnitude of the overall shear modulus is also well estimated, with a maximum relative error of 22% for the non corrected estimate and 4% for the corrected result.

The estimate of the overall shear modulus as a function of the volume fractions in both the UD and the foam core is illustrated on Fig. (7). It is readily observed that:

- the overall shear modulus is sensitive to the volume fraction of through-thickness reinforcement c_{H2} ;
- the overall shear modulus is not sensitive to the volume fraction within the UD c_{H1} (the four curves are basically indistinguishable). In fact, a

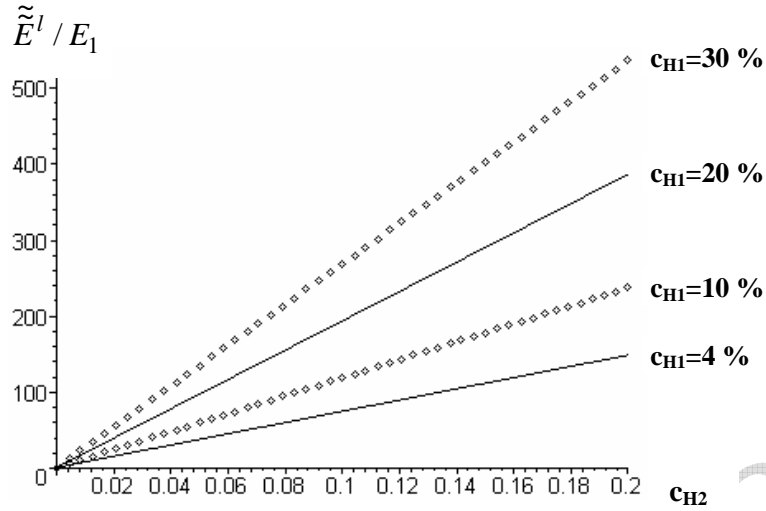


Figure 5. Estimate of the overall longitudinal Young's modulus \tilde{E}^l for different volume fractions c_{H1} within the UD.

differential calculus on Eq. (21) shows that an increase of the shear modulus of the UD does not imply a significant increase of the overall shear modulus (all other parameters being fixed otherwise). Also, note that an increase of the volume fraction within the UD implies a rather small increase of the shear modulus of the UD: in the case of a 20% increase (from 10% to 30%), the shear modulus of the UD increases by 40% while the Young's modulus increases by 130% approximately;

- once again, a significant increase of the property can be obtained.

4.3.3 Remark 1

The fact that the prediction of the overall shear modulus seems to be more accurate compared to the estimate of the effective Young's modulus may be explained by noticing that:

- basically, the micromechanical modelling does not integrate the effect of the skins, which may not be neglected in the case of a compression test;
- also, the estimate of the overall Young's modulus is highly sensitive to the volume fraction within the UD and thus, the difference between experimental and simulated curves may be due to volume fraction fluctuations (we recall that a mean value was considered in the model). This point will be discussed in section (5).

**Effective transverse
shear modulus, in MPa**

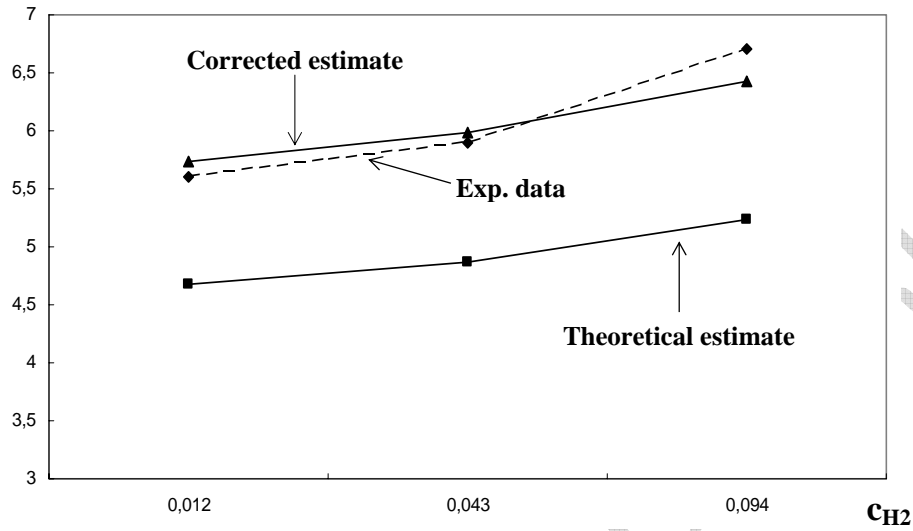


Figure 6. Comparison between exp. data and micromechanical predictions. Case of the overall transverse shear modulus $\tilde{\mu}^t$.

4.3.4 Remark 2

We note that for a given elastic property, and especially in the case of the overall transverse shear modulus (which is critical for sandwich core materials), the analysis carried out in this study (see sections (4.3.1) and (4.3.2)) shows that the parameter r_T is almost independent from the number of observations N (for instance, in the case of the overall transverse shear modulus, the index has a standard deviation less than 4%) and close to the unit. This means that:

- the variation of the elastic properties is correctly predicted ;
- only a few experimental measurements may be used for correcting the simulated results.

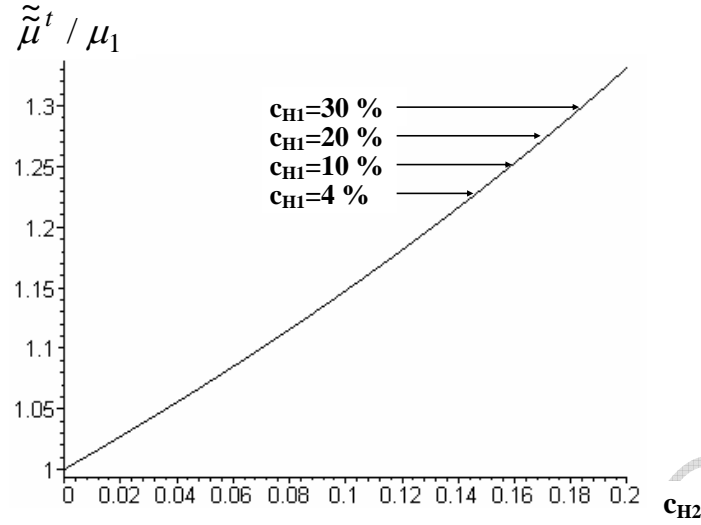


Figure 7. Estimate of the overall transverse shear modulus $\tilde{\mu}^t$.

5 On the influence of fiber volume fraction in the through-thickness reinforcements

5.1 Microstructural analysis

Several micrographic pictures have been realized on the UD reinforcing the foam core. Figure 8 shows that the needles carrying the fibers within the foam, that will create the UD during the resin injection, induces high discrepancies from one UD to another. In particular, it can be seen that the fiber volume fraction varies and that the UD are basically resin-rich regions. Further ex-

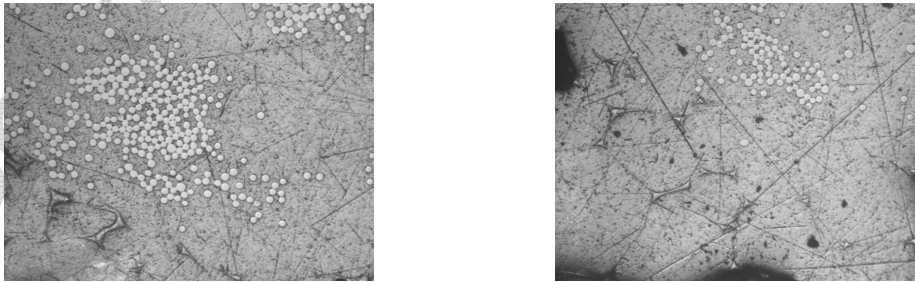


Figure 8. Example of UD cross-section micrographies (glass fibers appear white and resin appears grey)

perimental analysis of the fiber volume fraction within the through-thickness reinforcement clearly shows the randomness of this quantity, mainly due to

the randomness of the mat as well as to the manufacturing process itself. The aim of this section is then to construct a suitable parametric probabilistic model associated to such a random volume fraction, as well as to study, by means of Monte-Carlo numerical simulations, the influence of this uncertainty on the overall mechanical behavior (note that results will be provided only in the case of the longitudinal Young's modulus, which is shown to be the most sensitive parameter).

5.2 Construction of a parametric probabilistic model

Let $c(\theta) = c_{H_1}(\theta)$ be the random volume fraction under consideration (the symbol θ denotes the randomness of the quantity and is dropped hereafter for the sake of simplicity), defined on a probability space $(\mathcal{A}, \mathcal{F}, P)$. Its probability distribution P_c , such as $P_c(dc) = p_c(c) dc$, is then defined by a probability density function $p_c(c)$ defined on \mathbb{R} , with respect to the Lebesgue measure dc . The construction of the probability density function is achieved using the Maximum Entropy Principle (M.E.P.; see for instance [8] [12] [13] for a general overview). We recall that such a construction is only based on the available information and thus, no bias is introduced in the estimation of the probability distribution. The mean and standard deviation, denoted by m_c and σ_c respectively, are determined from usual mathematical statistics and are estimated from a set of 100 samples. For this purpose, the samples are classically burnt and weighed twice, before and after the calcination. This yields two constraints on the two first statistical moments, denoted by m_1 and m_2 respectively. We further specify the support of the distribution, defined as:

$$S = \text{Supp}(c(\theta)) = [0, 1] \quad (26)$$

Thus, the *available information* can be summarized as follows:

- the support S of the distribution is known: $c \in [0, 1]$ almost surely;
- the random variable c is of second order (that is $E\{c^2\} < +\infty$, where E denotes the mathematical expectation);
- the two statistical moments m_1 and m_2 are known.

Finally, let us recall the normalization condition for the density function:

$$\int_{\mathbb{R}} p_c(x) dx = 1 \quad (27)$$

Then, it can be shown that the probability density function, constructed using the M.E.P., takes the form:

$$p_c(x) = \mathbb{I}_S(x) \exp(-\lambda_0 - x\lambda_1 - x^2\lambda_2) \quad (28)$$

where $\mathbb{I}_S(x)$ is the indicator function ($\mathbb{I}_S(x) = 1$ if $x \in S$ and $\mathbb{I}_S(x) = 0$ otherwise) and the Lagrange multipliers $(\lambda_0, \lambda_1, \lambda_2) \in \mathbb{R}^3$ are such that they minimize the strictly convex functional $(\lambda_0, \lambda_1, \lambda_2) \rightarrow H(\lambda_0, \lambda_1, \lambda_2)$ defined as:

$$H(\lambda_0, \lambda_1, \lambda_2) = \lambda_0 + \lambda_1 m_1 + \lambda_2 m_2 + \int_S \exp(-\lambda_0 - x\lambda_1 - x^2\lambda_2) dx \quad (29)$$

Such an optimization problem can be solved by using usual techniques, such as the Conjugate Gradient method. Figs. (9) and (10) show the plots of the probability density function and the cumulative distribution function respectively.

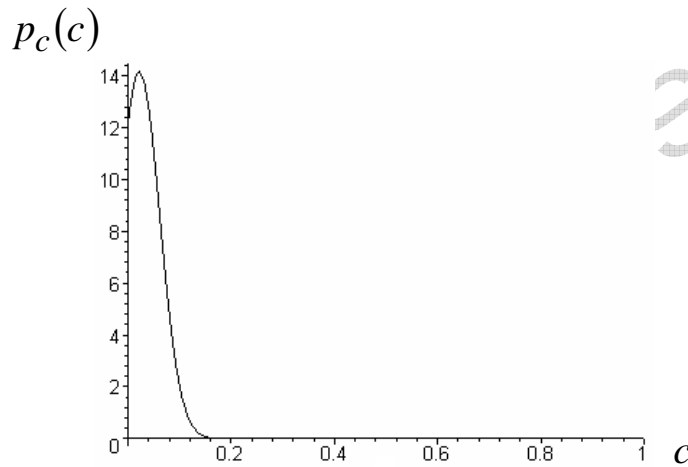


Figure 9. Probability density function of the random volume fraction.

5.3 Stochastic solver

Monte-Carlo numerical simulations [11] are used for assessing some statistical properties of the overall mechanical response. The methodology is classical and is summarized below:

- generate the random vector \underline{U} , of length N and such as each component $U^{(k)}$, $k = 1..N$, is uniformly distributed between 0 and 1;
- compute the random vector \underline{c} corresponding to the volume fraction c by using, for each component $c^{(k)}$, an inverse transform:

$$\underline{c}^{(k)} = F_c^{-1}(\underline{U}^{(k)}) \quad (30)$$

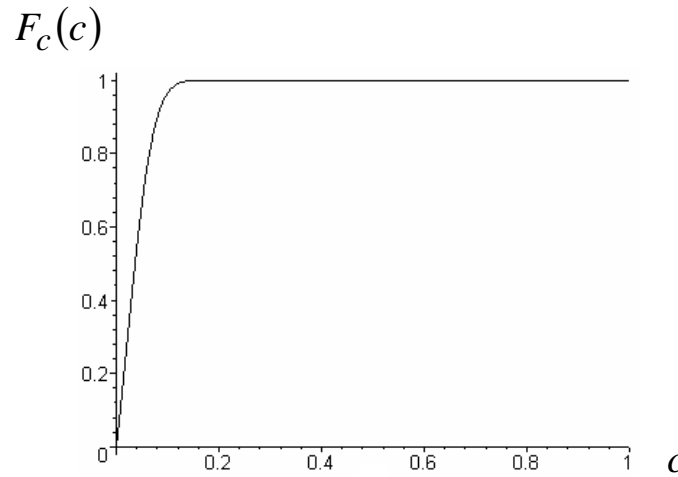


Figure 10. Cumulative distribution function of the random volume fraction.

where F_c is the cumulative distribution function of the random volume fraction;

- compute the vector $\tilde{\underline{E}}$ corresponding to the longitudinal Young's modulus by using the micromechanical formulations;
- perform the statistical analysis.

The properties assessed by 100 000 Monte-Carlo simulations (the number of simulations is controlled by the convergence of the first to the fourth order statistical moments) are listed in table (4) (volume fraction in UD's within the foam core: $c_{H_2} = 4.3\%$). The convergence of the mean, standard devia-

Min: 180.9 MPa
Max: 763.4 MPa
Median: 290.6 MPa
1st Qu.: 236.4 MPa
3rd Qu.: 355.3 MPa
Mean: 303.2 MPa
CV: 27.6 %

Table 4

Properties of the random overall longitudinal Young's modulus.

tion, skewness and kurtosis coefficients are illustrated in Figs. (11) and (12) (note that the values are basically normalized by the converged results). As expected, it is readily seen that the overall longitudinal Young's modulus is

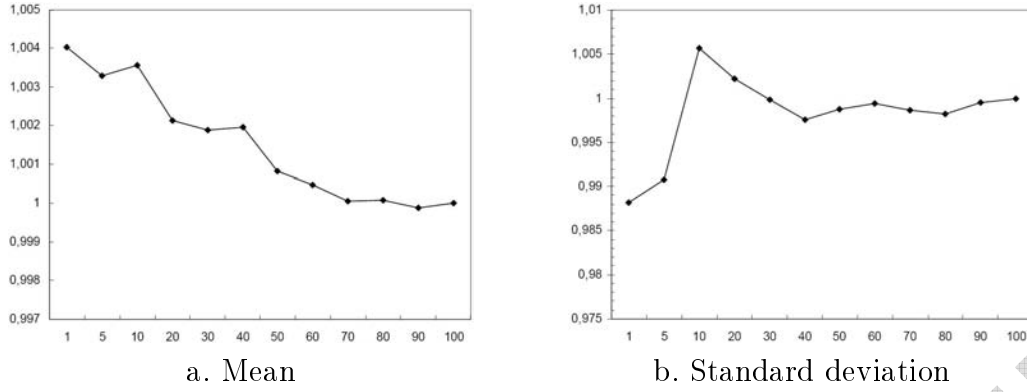


Figure 11. Convergence rates of the mean and standard deviation (abscissa $\times 10^3$: number of Monte-Carlo simulations).

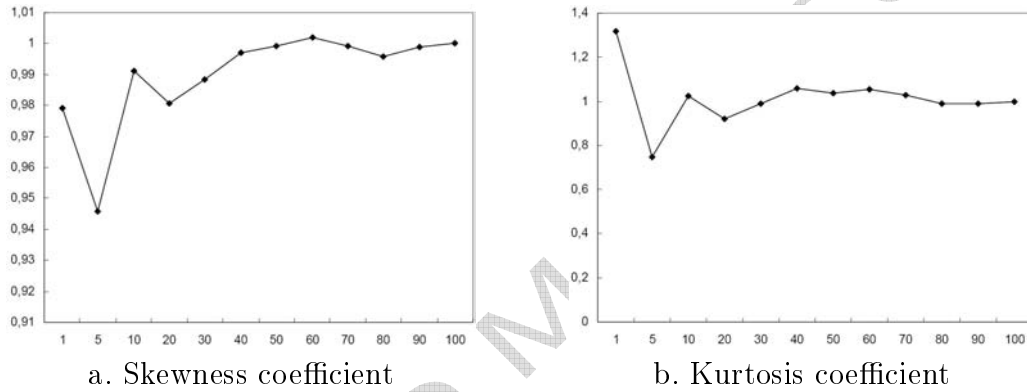


Figure 12. Convergence rates of the skewness and kurtosis coefficients (abscissa $\times 10^3$: number of Monte-Carlo simulations).

highly dispersed, with an inter-quartile deviation $IQD = 59.45 \text{ MPa}$. It is worth noticing that the stochastic overall longitudinal Young's modulus has a finite second moment ($E \{ \tilde{E}^2 \} < +\infty$) and is then, as expected, of second-order. Figs. (13) and (14) show the plots of the probability density function and the empirical cumulative distribution function of the overall longitudinal Young's modulus respectively.

Remark: note that the random volume fraction may not be considered as homogeneous over the composite part and thus, may be modeled by considering a random field (see [12]). However, such an analysis can only be performed within a computational framework and is beyond the scope of this study. It then becomes straightforward that the extreme values (say, out of the interquartile range) obtained here are meaningless, as some kind of balancing between strongly and weakly reinforced UD's may occur in reality.

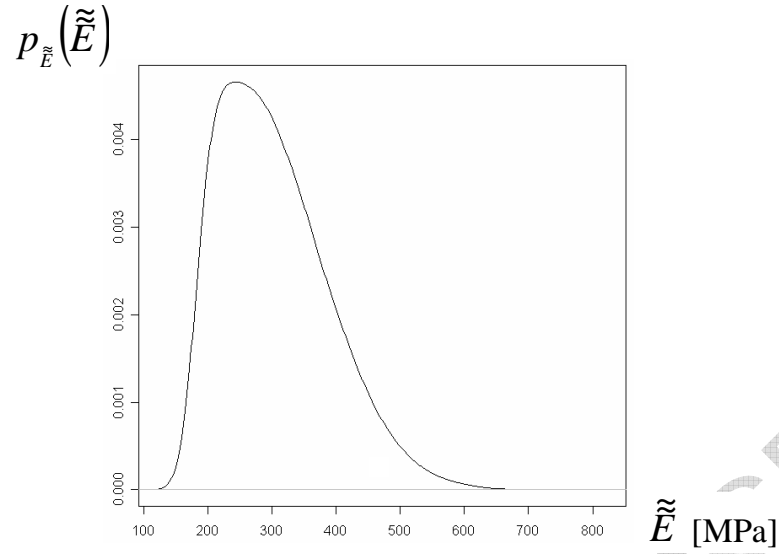


Figure 13. Probability density function of the overall longitudinal Young's modulus.

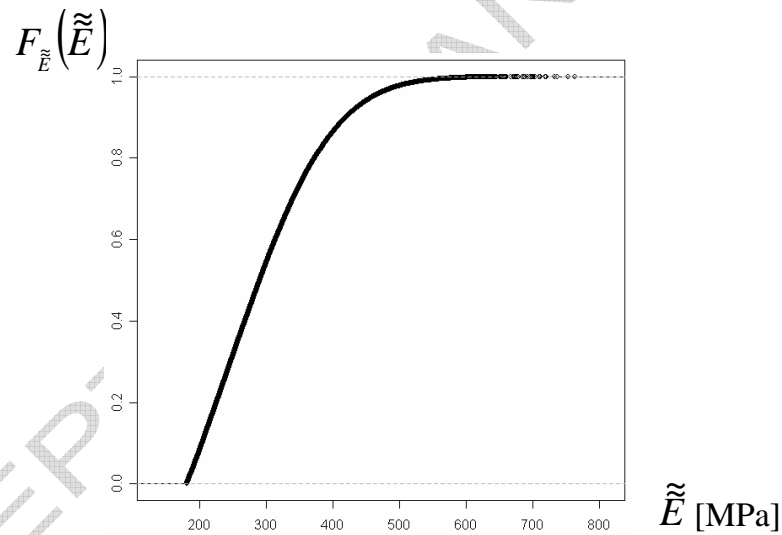


Figure 14. Empirical cumulative distribution function of the overall longitudinal Young's modulus.

6 Conclusion

The Napco[®] technology is a patented process that strengthens transversally foam core with fiber yarns taken from facings in sandwich assembly. In this study, we investigate the potential of this technology by means of a microme-

chanical analysis based on the Mori-Tanaka scheme. Comparisons between predictions and experiments are discussed and basically show the efficiency of the micromechanical modelling which can also be generalized to other configurations (for instance, for other distributions and/or orientations of the through-thickness reinforcements). The approach allows one to define easily both material and process parameters to tailor sandwich panel to specific core-related mechanical requirements. Furthermore, the randomness of the volume fraction within the through-thickness reinforcements is clearly shown and integrated using a parametric probabilistic model, Monte-Carlo numerical simulations being used as the stochastic solver. Such a modelling basically establishes a link between the randomness of the manufacturing process (here, the Napco[®] technology) and the uncertainties of induced mechanical properties. This information is of great help when designing and qualifying structures and can also be used in order to optimize the process itself. Finally, it is shown that such a technology can produce composite reinforced foam core with a significant improvement of the mechanical properties, and in particular the longitudinal Young's modulus as well as the transverse shear modulus.

References

- [1] Bannister, M.K., Braemar, R., Crothers, P.J. "The mechanical performance of 3D woven sandwich composites", *Composite Structures*, Vol.47, No. 1-4, pp. 687-690, 1999.
- [2] Benveniste, Y. "A new approach to the application of Mori-Tanaka's theory in composite materials", *Mechanics of Materials*, Vol. 6, pp. 147-157, 1987.
- [3] Bornert, M., Bretheau, T., Gilormini, P. (Eds.) "Homogenization in Mechanics of Materials", Iste Publishing Company, 2006.
- [4] Christensen, R. M. "Mechanics of Composite Materials, Rev. Ed.", Dover Publications, 2005.
- [5] Hosur, M. V., Abdullah, M., Jeelani, S. "Manufacturing and low-velocity impact characterization of hollow integrated core sandwich composites with hybrid face sheets", *Composite Structures*, Vol. 65, No.1, pp 103-115, 2004.
- [6] Lascoup, B., Aboura, Z., Khellil, K., Benzeggagh, M. "On the mechanical effect of stitch addition in sandwich panel", *Composites Sciences and Technology*, Vol.66, No. 10, pp. 1385-1398, 2006.
- [7] Mori, T. and Tanaka, K. "Average stress in matrix and average elastic energy of materials with misfitting inclusions", *Acta Metall.* 21, pp. 571-574, 1973.
- [8] Papoulis, A. "Probability, Random Variables, and Stochastic Processes, Third Edition", McGraw-Hill, 1991.

- [9] European patent n EP 0 594 700 B1
- [10] Potluri, P., Kusak, E., Reddy, T.Y. "Novel stitch-bonded sandwich composite structures", *Composite Structures*, Vol. 59, No.2, pp 251-259, 2003.
- [11] Rubinstein, R.Y. "Simulation and the Monte-Carlo Method", John Wiley and Sons, New-York, 1981.
- [12] Schuëller, G. I., et al. "A State-of-the-Art Report on Computational Stochastic Mechanics", *Probabilistic Engineering Mechanics*, Vol. 12 (4), pp. 197-321, 1997.
- [13] Soize, C. "A nonparametric model of random uncertainties for reduced matrix models in structural dynamics", *Probabilistic Engineering Mechanics*, Vol. 15, pp. 277-294, 2000.
- [14] Vaidya, U.K., Nelson, S., Sinn, B., Mathew, B. "Processing and high strain rate impact response of multi-functional sandwich composites", *Composite Structures*, Vol. 52, No. 3-4, pp. 429-440, 2001.
- [15] Walpole, L.J. "On the overall elastic moduli of composite materials", *Journal of Mechanics and Physics of Solids*, Vol. 17, pp. 235-251, 1969.